Korean J. Chem. Eng., **20**(5), 934-941 (2003)

Effect of Evaporation Temperature on the Crystalline Properties of Solution-Cast Films of Poly(vinylidene fluoride)s

Kwang Man Kim†, Woo Sung Jeon*, Nam-Gyu Park, Kwang Sun Ryu and Soon Ho Chang

Power Source Devices Team, Basic Research Lab., Electronics & Telecommunications Research Institute (ETRI),
161 Gajong, Yusong, Daejeon 305-350, Korea
*Department of Chemistry and Center for Smart Supramolecules,
Pohang University of Science and Technology (POSTECH), Pohang 790-784, Korea
(*Received 17 September 2002 • accepted 29 May 2003*)

Abstract−The crystalline properties of poly(vinylidene fluoride) (PVdF) and its copolymer films, prepared from the solvent (*N*-methyl-2-pyrrolidone) evaporation at different temperatures and subsequent slow cooling to ambient temperature, were investigated by using polarized optical microscopy, differential scanning calorimetry, wide-angle X-ray diffractometry, and Fourier-transform infrared spectroscopy. The results can provide helpful data for determining the optimal processing conditions of PVdFs as the polymer binder materials in making the electrodes of rechargeable lithium batteries. The morphology analysis gives useful information that the residual solvent remaining after the evaporation shows distinguishable amounts with respect to the temperature regions dividing by the crystallization (T_c) and melting (T_m) points of original PVdF samples. It is also proved that smallest spherulitic state coexisting with dominant α- and minor γ-phase crystals, simultaneously showing the lowest heat of fusion (e.g., the lowest crystallinity), can be obtained when the solvent is evaporated at a temperature between T_c and T_m. Letting the minor γ-phase crystals exist by controlling the evaporation temperature like this can be one of the best drying (evaporation) conditions of PVdF-containing slurry in lithium rechargeable battery system.

Key words: Poly(vinylidene fluoride)s, Crystalline Properties, *N*-Methyl-2-pyrrolidone, Evaporation Temperature

INTRODUCTION

During the last several decades, poly(vinylidene fluoride) (PVdF) has been known as a very versatile polymer material because of its many applications, especially based on its ferro-, pyro-, piezoelectric properties. Such properties could have been understood by the reflections of various crystalline polymorphisms exhibited under different conditions. Entering the 1990s, the usage of PVdF was expanded to a polymer binder material in the field of rechargeable lithium batteries, especially in lithium-ion battery (LIB) because PVdF sufficiently satisfies many requirements for binder material such as strong thermal resistance, high volumetric efficiency with small weight, and chemical stability against electrolyte solution. These features of PVdF have been confirmed by many Japanese battery-makers [Omaru et al., 1995; Itou et al., 1995; Ito et al., 1997; Kita et al., 1997], where PVdF dissolved in *N*-methyl-2-pyrrolidone (NMP) has proven to be the most favorable system of polymer binder solution in LIB production.

The electrode of LIB can be prepared by drying (evaporating the solvent) the wet-coated sheet that consists of electrically active materials dispersed in the polymer binder solution. The drying condition may alter the crystal phase of PVdF that has probably an influence on the physical and chemical properties of the electrode film. In order to fabricate high quality electrodes, most basically needed is the information for the crystalline phase change of solution-cast PVdF film with the evaporation temperature (T_e). Extensive studies have been carried out for the crystalline phases of PVdF, which were obtained by melt-crystallization [Lovinger, 1980; Al-Raheil and Qudah, 1996; Prest and Luca, 1978; Sajkiewicz, 1999], solution-casting [Prest and Luca, 1978; Gregorio and Cestari, 1994; Benedetti et al., 1996; Bodhane and Shirodkar, 1997], thermoreversible gelation [Tazaki et al., 1997; Sato et al., 1998; Mal and Nandi, 1998], and monofilament fiber processing [Laroche et al., 1998]. Referring to an excellent review given by Lovinger [1981], four crystalline phases (α, β, γ, and δ) could be existing but mostly three phases (α, β and γ) may appear by solution crystallization during the preparation of LIB electrode. What phase appears or transforms into other phase depends on the crystallization temperature and annealing time. It may be also understood that β and δ phases do not contribute significantly to LIB performances since they are rather associated with piezo- and/or pyro-electrical properties.

The α-phase crystals frequently appear as dominant ringed spherulites, with which the minor β-phase crystals are also involved when crystallized at low temperature (<100 °C), or with which the γ-phase non-ringed spherulites when crystallized at high temperature (>155 °C) [Gregorio and Cestari, 1994; Sajkiewicz, 1999]. During high-temperature crystallization, the appearance of γ-phase crystals may be frequent by the prolonged annealing time, or partially accumulated by the transformation from α-phase. On the other hand, the PVdF as a polymer binder material in LIB electrodes should have an optimum crystalline phase, neither whole α- nor whole γ-phase. We have considered that the best crystalline phase would be, for instance, a large number of small spherulites (γ-phase) distributed widely over the entire range of electrode. The basis for this idea is that small spherulites (γ-phase) may be more effective than big ones

†To whom correspondence should be addressed.
E-mail: kwang@etri.re.kr

(α-phase) in binding active material particles in the preparation of LIB electrode. In general, such a γ-phase crystalline state is actually difficult to achieve from simple PVdF/NMP system because the α-crystals appear dominantly under usual evaporation condition. In the actual LIB electrode system, however, the PVdF crystalline properties should be carefully investigated on the cast film because the film forms from the slurry consisting of not only PVdF/NMP solution but also active material particles (e.g., carbon, cokes, or graphite for negative electrode; $LiCoO_2$, $LiMn_2O_4$, or $LiNiO_2$ for positive electrode).

As a preliminary step for that purpose, the present work examines the effect of T_e, not crystallization temperature, on the crystalline phases of PVdF/NMP solution-cast film on a glass plate. The results will provide basic, but important, information in optimizing the T_e with best crystalline phases adequate to apply in the preparation of LIB electrode sheet.

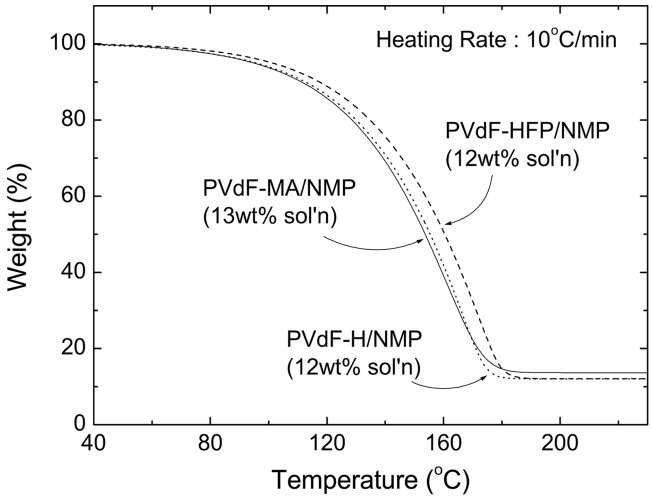

Fig. 1. Thermogravimetric analysis results for three PVdF solution samples measured at the scan rate of 10 °C/min.

EXPERIMENTAL

Three kinds of PVdF sample were used: PVdF-H, P(VdF-HFP) (Elf Atochem N.A.), and P(VdF-MA) (Kureha Chem. Ind.). PVdF-H is a PVdF homopolymer powder that is generally used as polymeric binder material in LIB industry. P(VdF-HFP) is a copolymer powder of vinylidene fluoride and hexafluoropropylene (88 : 12 in weight basis). P(VdF-MA) is a copolymer of vinylidene fluoride and maleic acid monoester (99 : 1 in weight basis), which is developed to enhance the adhesion between active material particles and metal foil (current collector). The P(VdF-MA) was provided from the supplier as a 13 wt% polymer solution dissolved in NMP. Molecular weights and some thermal properties of samples were summarized in Table 1.

First, thermogravimetric tests (SDT2560, TA Instrument Co.) for some samples with different polymer compositions were carried out in order to examine the evaporation trend of solvent NMP with increasing the temperature (heating rate 10 °C/min). And, 12 wt% polymer solutions dissolved in NMP (Aldrich) were also prepared for the samples of PVdF-H and P(VdF-HFP). The P(VdF-MA)/NMP solution was used as received from the supplier. Polymer solution was applied at room temperature on a cleaned glass plate, which was promptly spread by a doctor blade with a fixed gap of 300 μm. Immediately, the coated plate was quickly moved to a mechanical convection oven (Model 625, Precision Scientific Co.) keeping a pre-specified temperature. The temperature specified was varied as 110 (below T_c), 130 (below T_c), 150 (between T_c and T_m), 170 (near T_m), and 190 °C (above T_m) for PVdF-H and P(VdF-MA) where T_c and T_m denoted the crystallization and melting temperatures, respectively. Similarly, the specified temperature for the P(VdF-HFP) copolymer sample was also varied as 90 (below T_c), 110, 130 (between T_c and T_m), 140 (near T_m), and 150 °C (above T_m). After keeping for 10 min in the oven, the sample was exposed to air and slowly cooled down to ambient temperature to give the final PVdF film cast on glass plate. Slow cooling was made to give a close condition to real LIB electrode production.

The films were in good adhesion states but, in a sense of peeling off by hand, the resistance to the peeling was in the order of P(VdF-MA)>P(VdF-HFP)>PVdF-H. The films peeled off carefully from the glass plate were within the thickness range of 60-100 μm. Calorimetric analyses were carried out for the films at a heating rate of 10 °C/min by a differential scanning calorimeter (DSC, du Pont Model 2010 System with Model 910 Analyzer). A polarized optical light microscope (Leitz Model Laborlux 12 Pols, ×500), equipped with a camera and an automatic exposure controller, was used to obtain the micrographs for the morphologies of samples cooled down to room temperature. Wide-angle X-ray diffraction (XRD) measurements were also carried out by using a Rigaku X-ray generator which recorded diffraction patterns by Cu-Kα_1 radiation with wavelength λ=0.15406 nm. Chemical stability and crystalline phase change, which might occur at different T_e, were also investigated by a Fourier-transform infrared (FT-IR) spectrometer (Bomem MB-100) with the wavelength resolution of 4 cm^{-1}.

Table 1. Molecular characteristics and some thermal properties of PVdF samples used

	PVdF-H	P(VdF-HFP)	P(VdF-MA)
Number-averaged molecular weight	177,900	210,800	>500,000
Weight-averaged molecular weight	517,400	822,500	
Glass transition temperature T_g (°C)	−43.9	−35.4	
Melting temperature T_m (°C)	168.20*	141.54*	172±1
Crystallization temperature T_c (°C)	140.94*	105.72*	139±1
Heat of fusion ΔH_m (J/g)	58.22*	32.30*	
Heat of crystallization ΔH_c (J/g)	−44.28*	−23.98*	

*Directly measured using DSC (heating rate of 10 °C/min).

RESULTS AND DISCUSSION

1. Solvent Evaporation

Fig. 1 shows weight-decreasing pattern of PVdF solutions with the increase in temperature. NMP in the solution starts to evaporate at about 50 °C, much lower than the boiling point of pure NMP (~204 °C). Nearly all quantity of solvent NMP evaporates when arriving at about 180 °C. More than 90% of NMP disappears within the range of 100-170 °C. At about 160 °C, the highest rate of evaporation appears, at which the maximum rates of weight loss are 18.2 (for 12 wt% PVdF-H/NMP) and 19.0 wt%/min [for 13 wt% P(VdF-MA)/NMP]. 12 wt% P(VdF-HFP)/NMP sample exhibits a similar trend of highest evaporation rate (20.3 wt%/min) but at the slightly elevated temperature of ~170 °C. The elevated temperature may be due to the fact that small amount of flexible hexafluoropropylene spacer in the copolymer chain structure has higher affinity with the solvent molecules than vinylidene fluoride unit and thus the solvent evaporation may be slightly delayed. The evaporation can only occur just after the affinity interaction disappears, and thus the evaporation rate does not depend on the affinity.

In real process of LIB electrode making, however, such high temperature does not need to evaporate the solvent NMP because the thermogravimetric curve of active mass-containing slurry shifts to lower temperature region than the case of containing polymer binder only [Sugawara, 1998]. The determination of T_e to remove the solvent should be optimized by considering many features associated with solvent evaporation, polymer binder properties, and slurry

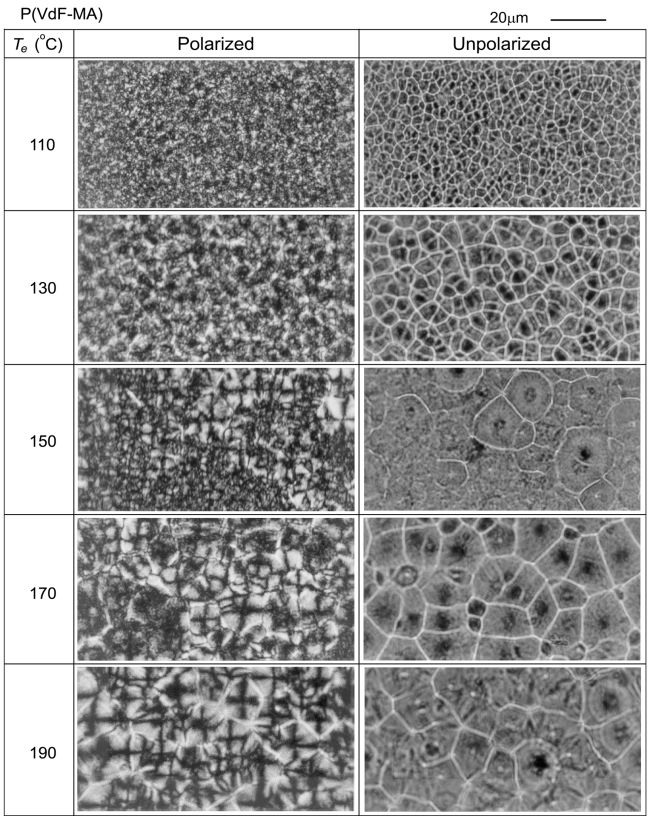

Fig. 3. Surface images (polarized and unpolarized) of P(VdF-MA) films with the variation of evaporation temperature.

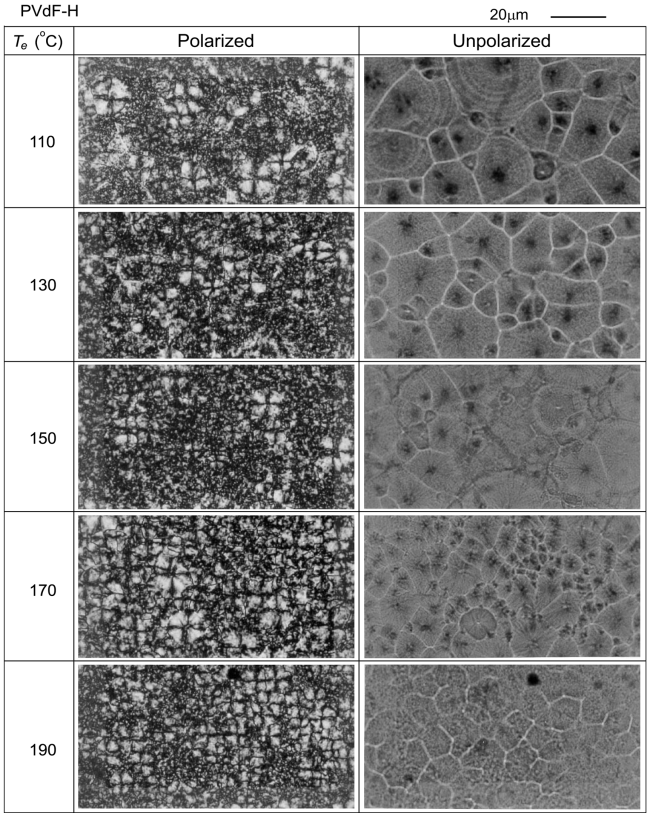

Fig. 2. Surface images (polarized and unpolarized) of PVdF-H films with the variation of evaporation temperature.

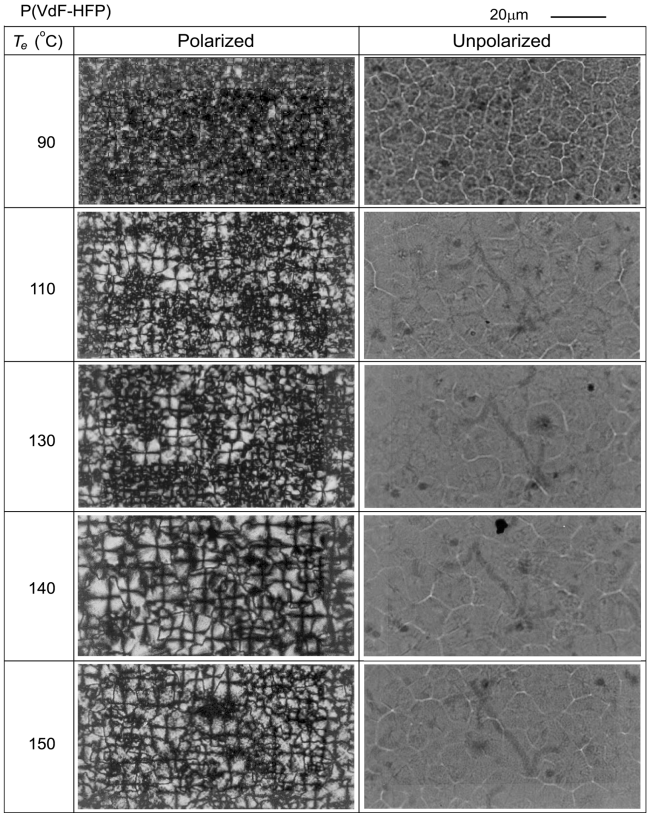

Fig. 4. Surface images (polarized and unpolarized) of P(VdF-HFP) films with the variation of evaporation temperature.

characteristics.

2. Morphology

Unlike other films quenched to interrupt crystallization, the present films suffer slow cooling under atmospheric environment and thus they may possess different memories of thermal history on crystal phases. That is, due to the same condition of slow cooling after the evaporation, the sample evaporated at higher temperature has the memory of thermal history, which is embedding the memory of other sample evaporated at lower temperature. Figs. 2-4 show both polarized and unpolarized micrographs of PVdF samples, which are taken at ambient temperature but via different T_e's. The polarized picture may give us information on crystal morphology (e.g., size, shape, and distribution), whereas the unpolarized one on macroscopic surface state after the solvent evaporation (e.g., hexagonal convection cell and/or residual solvent). The surface morphology seems to be somewhat complex, but we can capture some significant patterns with increasing the T_e if careful observation is provided.

For the PVdF homopolymer sample obtained through the evaporation at 110 °C (see upper part of Fig. 2), big spherulites of ~10 μm in average size are distributed with a mean distance of ~10 μm, and therein so many tiny crystals and amorphous regions scattered. As the T_e is increased, spherulites are getting smaller until reaching T_e=150 °C and then grow up to the comparable size when arriving at T_e=190 °C, but tiny crystals scattered among the big spherulites are seen to be increasing in their size slightly and constantly. Consequently, the sample evaporated at higher temperature than T_m may include many superimposing spherulites that have been contributed by the shrinkage of big spherulites as well as the growth of tiny crystals. Also, the average size of crystals seems to have a minimum when the T_e lies between T_c and T_m.

Unpolarized pictures in Fig. 2 show many convection cells with various sizes and shapes. The residual solvent (NMP) component remained after the evaporation can be also seen apparently as black spots in the center of convection cell. Ideal evaporation in the situation of heating homogeneously the glass plate may produce hexagonal convection cells (Bénard cells) caused by surface tension gradient [Koschmieder, 1993]. Non-hexagonal cells appearing here can be regarded as the arbitrarily formed products from an impact between the expanding circular ripples by solvent convection gradient trace and the surface tension (or adhesion at the onset of film formation) of polymer chain with glass plate. Big convection cell may appear by prolonged convection time when the instant evaporation rate is slow. In case of low T_e below T_c, thus, comparatively large convection cells appear and become smaller with increasing T_e. Compared with the polarized image, in addition, it can be seen that the boundary of the convection cell, as a line defect (a sort of disclination), plays a role of nucleating agent to grow the spherulites. These qualitative trends, described above for spherulites (in polarized image) and convection cells (in unpolarized image), are also revealed in the case of using P(VdF-HFP) film, as shown in Fig. 4. The morphology analysis can give important information that the inclusion of flexible spacer unit lowers the crystallinity of polymer chains and thereby the decreases in the referencing temperatures such as T_c and T_m.

In Fig. 3 for P(VdF-MA) as the best case of adhering with glass plate, the growth of spherulites is obviously seen as T_e increases, but the minimum in average size of them is not shown in the region between T_c and T_m, different from the case of PVdF-H. It is rather observed that the distribution of grown spherulites is localized with increasing T_e and then they dominate the entire film surface and even superpose each other to give many distorted spherulites when evaporated at T_e higher than T_m.

On the other hand, convection cells are very small and contact closely with each other at low T_e below T_c, grow to a comparable size with the corresponding spherulites with increasing T_e, and then are saturated in their size at high T_e over T_m. Very small cells at low T_e are due to the dominance of surface tension (or adhesion) on glass plate, compared to the convection of solvent molecules; thus, an amount of residual NMP which is not evaporated remains in the center of the convection cell. Meanwhile, for the case of evaporating at high T_e above T_m, prolonged cooling permits large convection cells, but the dried surface formed by instant evaporation obstructs further evaporation of solvent on glass plate. This is another case of remaining residual NMP, which might be particularly caused by the film thickness (60-100 μm). Nonetheless, the P(VdF-MA) film obtained through the evaporation at the region of $T_c<T_e<T_m$ contains the minimum amount of residual NMP and it may be a criterion for the determination of optimal drying condition.

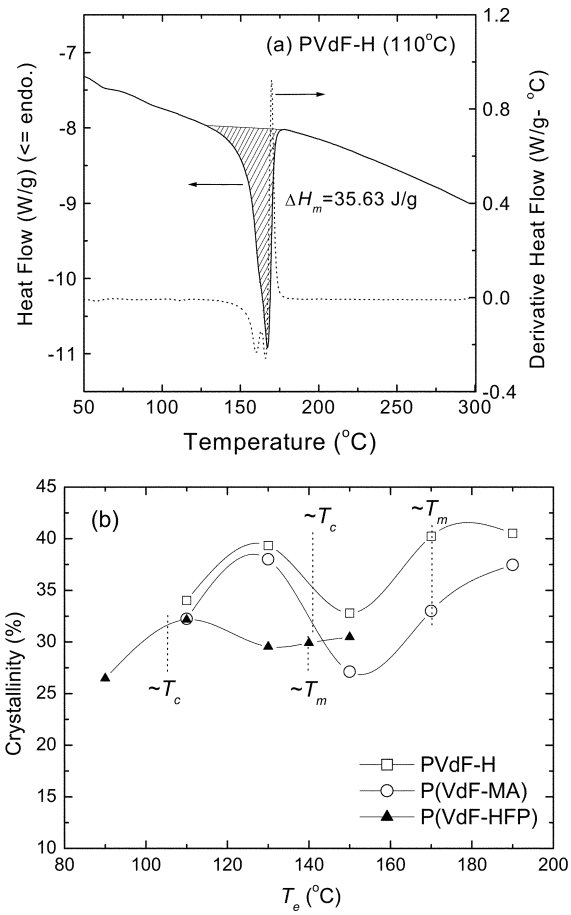

Fig. 5. (a) Data analysis example for the ΔH_m (heat of fusion) calculation of the PVdF-H film obtained by the evaporation at 110 °C, and (b) the crystallinity calculated from ΔH_m vs. evaporation temperature for the PVdF samples used.

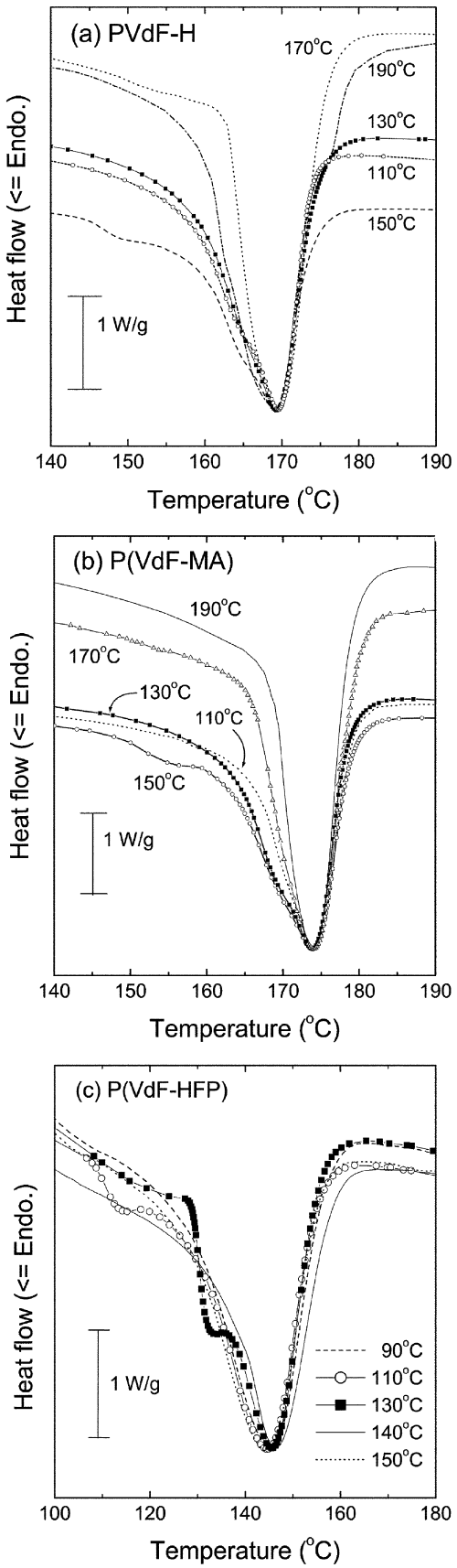

Fig. 6. DSC thermograms of the polymer films of (a) PVdF-H, (b) P(VdF-MA), and (c) P(VdF-HFP) films obtained through the evaporation at various temperatures.

3. Thermal Property

A typical thermogram for the PVdF-H film evaporated at 110 °C is shown in Fig. 5(a) with its derivative curve to determine the baseline temperatures at which the instant value of the derivative curve becomes zero in the vicinity of the melting point. The heat of fusion ΔH_m may be calculated from the area consisting of the baseline and the melting curve. The crystallinity (%) of the film can also be calculated as $\Delta H_m/\Delta H_m^o \times 100$, where ΔH_m^o (≈104.7 J/g) denotes the heat of fusion for the pure α-phase crystal [Rosenberg et al., 1991]. The crystallinities for all the PVdF sample films, calculated by the above method, are shown in Fig. 5(b) with respect to the variation of T_e.

As T_e increases, all the PVdF sample films show similar trend of crystallinity: increase, decrease, and increase again or saturation. An emphasis should be put on the existence of minimum or a local minimal point in crystallinity, which occurs when evaporated at $T_c < T_e < T_m$. It seems that the minimum crystallinity comes from the smallest spherulites at this T_e range, as discussed in the morphology analysis, and then from the lowest ΔH_m. Crystals appearing at $T_e > T_m$ are larger ones suffering by recrystallization via the crystal melting, and those at $T_e < T_c$ are also larger ones formed by simple crystallization without passing through any characteristic temperature associated with crystal change. Thus, the recrystallization of partially melted and unmelted crystals results in the smaller spherulites appearing through the evaporation at $T_c < T_e < T_m$. It is noteworthy here that the crystal phases of α and γ might be associated with those spherulites, based on the fact that high temperature (~162 °C) crystallization gives α and γ phase crystals and low temperature (~155 °C) α-phase crystals [Sajkiewicz, 1999], and the temperature range of 155-162 °C is surely within $T_c < T_e < T_m$.

Fig. 6 shows DSC thermograms, putting the melting peak first in importance, for the PVdF sample films obtained after the evaporation and slow cooling. Unlike the case of isothermal crystallization, an endothermic peak at ~160 °C [for PVdF-H and P(VdF-MA) films] which might typically occur independent of T_c and annealing time [Prest and Luca, 1978; Sajkiewicz, 1999] is not observed. That can be done because the present study takes the other crystallization procedure followed by the solvent evaporation and subsequent cooling. Rather, what is emphasized is that melting points for all sample films, irrespective of the T_e, are nearly the same as those of original PVdF materials in the form of powder or solution, but just the intensities of endothermic peak corresponding to heat of fusion or crystallinity are differently observed, as discussed above. Here, it is difficult to determine exactly the kind of crystal phase for the endothermic peak, but it is expected from the morphology analysis that the distribution of α-phase crystals is dominant and γ-phase crystals play a minor role. Another emphasis should be put on the small endothermic peak at lower temperature than T_m for the case of evaporating at $T_c < T_e < T_m$, which is not observed in other temperature ranges of $T_e > T_m$ and $T_e < T_c$. The small peak is considered as a result from the melting of crystals formed from the amorphous phase during annealing (evaporation time) and the reorganized crystals during the slow cooling to room temperature [Al-Raheil and Qudah, 1996].

4. X-ray Diffraction Pattern

Fig. 7 shows the diffractograms obtained for the PVdF sample films and classified with respect to the evaporation temperature ranges

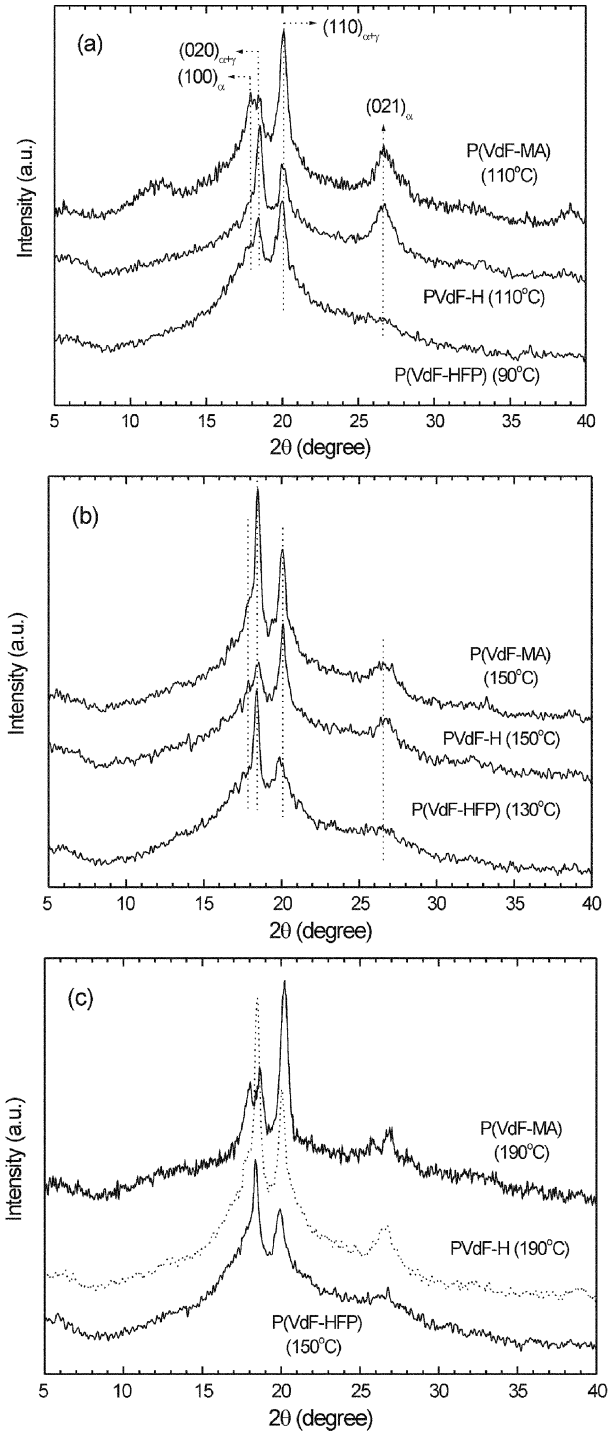

Fig. 7. XRD patterns for the PVdF sample films classified with respect to the evaporation temperature ranges of (a) $T_e<T_c$, (b) $T_c<T_e<T_m$, and (c) $T_e>T_m$. Same intensity scale is used for all diffractograms in the figure.

of $T_e<T_c$, $T_c<T_e<T_m$, and $T_e>T_m$. Compared with the pure α- and pure γ-phase crystals [Marand et al., 1988], all sample films manifest the slightly deviated diffractograms, as much as the amount of γ-phase crystals contained, from pure α-phase. In the pure α-phase, the reflections at 2θ=18.0, 18.6, 20.2, and 26.8° correspond to (100), (020), (110) and (021) planes, respectively. It has been also known

Table 2. Intensity ratio and crystal sizes determined from XRD analysis

Sample	T_e (°C)	$\frac{I(110)_{\alpha+\gamma}}{I(100)_\alpha}$	Crystal size (nm)*			
			L_{100}	L_{020}	L_{110}	L_{021}
PVdF-H	110	2.64	14.7	20.3	16.0	6.4
	130	3.30	7.2	26.2	16.6	6.9
	150	3.53	8.4	26.4	15.4	6.0
	170	3.38	8.6	26.1	17.6	5.8
	190	2.02	6.3	28.0	16.0	7.0
P(VdF-MA)	110	2.48	10.5	30.3	15.5	4.9
	130	3.00	6.3	27.9	16.7	7.0
	150	3.39	24.5	15.6	15.9	7.6
	170	3.15	10.0	27.4	18.2	6.7
	190	2.98	12.5	20.9	16.4	4.7
P(VdF-HFP)	90	2.27	5.8	26.9	13.6	-
	110	2.79	5.6	22.1	14.6	4.4
	130	2.66	5.5	25.9	10.4	4.6
	140	2.40	5.3	24.7	13.8	5.6
	150	1.53	5.8	28.1	14.1	5.1

*Calculated from the peak data at 2θ=18.0, 18.6, 20.2, and 26.8° for $(100)_\alpha$, $(020)_{\alpha+\gamma}$, $(110)_{\alpha+\gamma}$, and $(021)_\alpha$ planes, respectively.

that the reflections appearing at 2θ=18.0-20.7° might indicate some planes such as (020), (110), and (021) of γ-phase, together with those of α-phase. By following the analysis method of Marand et al. [1988], intensities of $(100)_\alpha$, $(021)_\alpha$, $(110)_{\alpha+\gamma}$ reflections are mainly concerned for discussing the change of crystal phases under different T_e conditions. All diffractograms obtained were fitted by Gaussian line shape regression to analyze peak properties and to determine the crystal sizes L_{hkl} corresponding to each reflection by using the Scherrer equation:

$$L_{hkl}=\frac{k\lambda}{\beta\cos\theta}$$

where L_{hkl} denotes the crystal size normal to hkl plane, k a factor equal to 0.89 [Voice et al., 1997], λ (=0.15406 nm) the wavelength of radiation beam used, β the halfwidth of peak determined by Gaussian line shape fitting, and θ the Bragg angle the peak appeared. Crystalline properties obtained by these analyses are summarized in Table 2.

As the T_e increases up to above T_m, the intensity of $(021)_\alpha$ decreases and then increases for PVdF-H and P(VdF-MA) films, whereas it shows no obvious change for P(VdF-HFP) film. The problem of P(VdF-HFP) is thought to be not significant because comparatively low crystallinity of P(VdF-HFP) film by the inclusion of amorphous HFP unit is easily expected. Rather, the increase in the intensity ratio $I(110)_{\alpha+\gamma}/I(100)_\alpha$, shown when the T_e raises up to $T_c<T_e<T_m$, is more important. According to Marand et al. [1988], the decreased $I(021)_\alpha$ and increased $I(110)_{\alpha+\gamma}/I(100)_\alpha$ (see Table 2) adequately verify the distribution of γ-phase crystals, and precisely the initially formed large α-phase spherulites as well as the nucleated small γ-phase crystals at later times.

Crystal sizes determined from the halfwidths of fitted peaks do not show a definite effect on the variation of T_e. Unfortunately, it is impossible to quantify accurately the reduction in crystal size at $T_c<$

$T_e<T_m$ by these analyzed data. This is due to the hopelessness of dividing $\alpha+\gamma$ mixture into each contribution. What the data can give us is just that, as expected, the crystals for L_{020} and L_{110} corresponding to the reflection peaks of $\alpha+\gamma$ mixtures are comparatively larger than those (L_{100} and L_{021}) of showing α-crystal only. One may say that the P(VdF-HFP) film evaporated at 150 °C, exhibits distinguishable crystal sizes of L_{100} (extended about twice) and L_{020} (reduced about a half) from the other cases of evaporating at different T_e's. We think that this change of crystal size is not remarkable enough to match with the entire trend of crystalline properties.

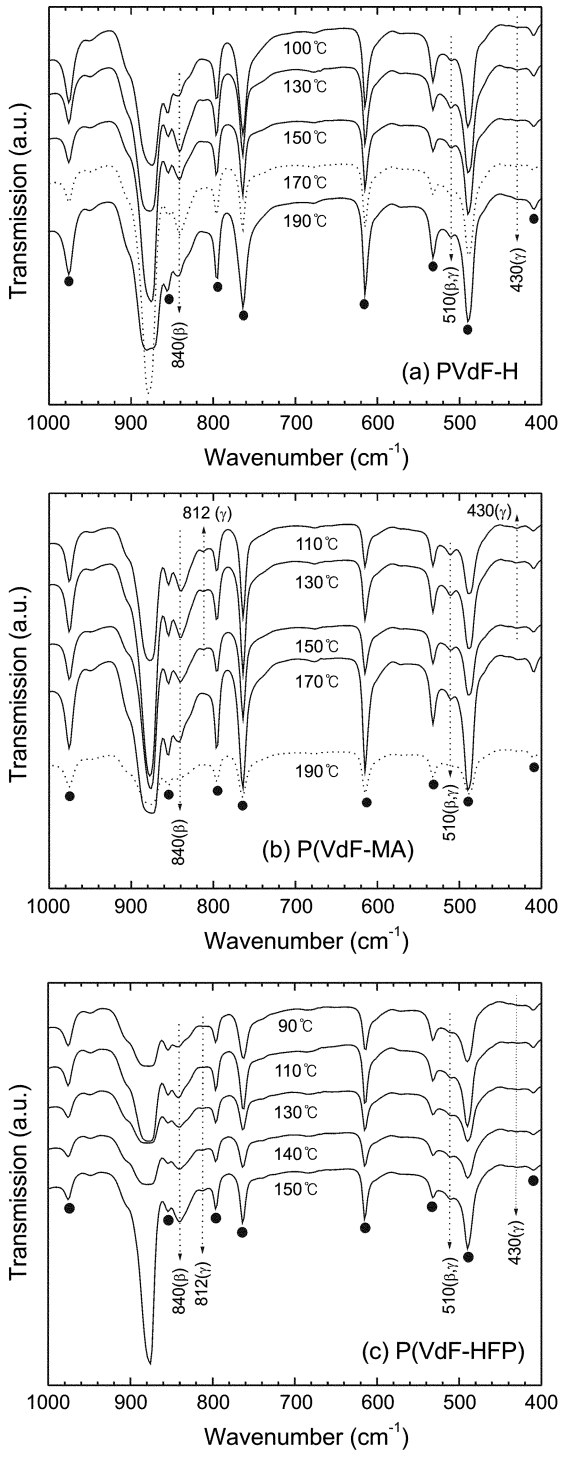

Fig. 8. FT-IR spectra of the polymer films of (a) PVdF-H, (b) P(VdF-MA), and (c) P(VdF-HFP) films obtained through the evaporation at various temperatures. Filled circles represent typical peaks (at 976, 855, 796, 765, 612, 531, 489 cm^{-1} from left) for α-phase spherulites.

5. FT-IR Spectra Analysis

The existence of γ-phase crystal can be also confirmed by FT-IR as well as other crystalline phases. Characteristic bands for various crystalline phases of PVdF have been reported by many authors [Prest and Luca, 1978; Gregorio and Cestari, 1994; Gregorio and Ueno, 1999; Eriguchi et al., 1999]: in summary, strong vibrational bands at 976, 855, 796, 765, 612, 531, 489, and 408 cm^{-1} correspond to α-phase; bands at 840, 510, 472, 468, and 420 cm^{-1} to β-phase; bands at 834, 812, 778, 510, 484, and 430 cm^{-1} to γ-phase. Fig. 8 shows the FT-IR spectra for the PVdF films obtained. Exclusively considering the dominant α-phase (filled circles), the presence of β- and γ-phase crystals is shown to be prominent. It is noteworthy that the effect of β-phase remains nearly constant for all films, represented by the bands at 840 (β) and 510 cm^{-1} (β, γ). This is probably due to the same exertion on the film by somewhat constant external field, e.g., same application of elongational force when the sample is treated to test. This agrees with the fact that the β-phase can be produced by the exertion of field force (e.g., elongation or electrical poling) from the PVdF/NMP solution system, according to the transformation relationship of the crystalline phases of PVdF samples [Lovinger, 1981]. Thus, consideration of β-phase can be excluded if careful treatment during sample preparation is provided. Meanwhile, the γ-phase is more apparently shown in P(VdF-MA) copolymer films than in PVdF-H and P(VdF-HFP), taking up the weak bands at 812 and 430 cm^{-1}. Though the precise distinction is difficult, the γ-phase signal of P(VdF-MA) film can be confirmed well, particularly for the cases of evaporating at $T_c<T_e$ (=150 °C)$<T_m$.

CONCLUDING REMARKS

As explained in the introduction, the emphasis on γ-phase crystal is for the enhancement of binding property of PVdF polymers in the production of LIB electrodes. Very small γ-phase crystals in the electrode often place or form at the edge of big α-phase spherulites and then play an intermediate role of connecting the crystalline and amorphous regions. The effects on the electrode properties, not only the binding but also the swelling by the electrolyte solution, can be highly enhanced by the inclusion of γ-phase crystals. From the above discussion, such γ-phase crystals were confirmed to be formed if the evaporation at $T_c<T_e<T_m$ was done. The present results can provide an optimal condition of preparing the γ-phase-containing PVdF films. Eventually, these can be used as a kind of prerequisite data in determining the best condition for producing PVdF γ-phase-containing electrodes of LIB.

REFERENCES

Al-Raheil, I. A. and Qudah, A. M., "Thermal Behavior and Annealing of Poly(vinylidene fluoride)," *Polym. Intern.*, **41**, 323 (1996).

Benedetti, E., Catanorchi, S., D'Alessio, A., Moggi, G., Vergamini, P., Pracella, M. and Ciardelli, F., "FTIR Microspectroscopy and DSC

Studies of Poly(vinylidene fluoride)," *Polym. Intern.*, **41**, 35 (1996).
Bodhane, S. P. and Shirodkar, V. S., "Change in Crystallinity of Poly (vinylidene fluoride) Due to Thermal Evaporation," *J. Appl. Polym. Sci.*, **64**, 225 (1997).
Eriguchi, T., Kamiya, H. and Endo, E. (Asahi Glass Co.), Jpn. Patent 1999-354163 (disclosed) (1999).
Gregorio, Jr. R. and Cestari, M., "Effect of Crystallization Temperature on the Crystalline Phase Content and Morphology of Poly(vinylidene fluoride)," *J. Polym. Sci. Part B: Polym. Phys.*, **32**, 859 (1994).
Gregorio, Jr. R. and Ueno, E. M., "Effect of Crystalline Phase, Orientation and Temperature on the Dielectric Properties of Poly(vinylidene fluoride) (PVDF)," *J. Mater. Sci.*, **34**, 4489 (1999).
Ito, S., Murata, T., Hasegawa, M., Bito, Y. and Toyoguchi, Y. (Matsushita Electric Co.), US Patent 5629109 (1997).
Itou, T., Teraji, K., Yoshinaga, N., Harada, S., Neguro, K. and Mori, K. (Sanyo Electric Co.), US Patent 5380606 (1995).
Kita, F., Higashiguchi, M., Murakami, K. and Kawakami, A. (Hitachi Maxell Ltd.), US Patent 5691084 (1997).
Koschmieder, E. L., "Bénard Cells and Taylor Vortices," Cambridge University Press (1993).
Laroche, G., Lafrance, C.-P., Prud'homme, R. E. and Guidoin, R., "Identification and Quantification of the Crystalline Structures of Poly (vinylidene fluoride) Sutures by Wide-Angle X-Ray Scattering and Differential Scanning Calorimetry," *J. Biomed. Mater. Res.*, **39**, 184 (1998).
Lovinger, A. J., "Crystallization and Morphology of Melt-Solidified Poly(vinylidene fluoride)," *J. Polym. Sci. Polym. Phys. Ed.*, **18**, 793 (1980).
Lovinger, A. J., "Poly(vinylidene fluoride)," Developments in Crystalline Polymers, Basset, D. C., ed., Vol. 1. Applied Science Pub., Chap.5 (1981).
Mal, S. and Nandi, A. K., "A Thermodynamic Study on the Thermoreversible Poly(vinylidene fluoride) Gels in Acetophenone, Ethyl Benzoate, and Glyceryl Tributyrate," *Langmuir*, **14**, 2238 (1998).
Marand, H. L., Stein, R. S. and Stack, G. M., "Isothermal Crystallization of Poly(vinylidene fluoride) in the Presence of High Static Electric Field. I. Primary Nucleation Phenomenon," *J. Polym. Sci. Part B: Polym. Phys.*, **26**, 1361 (1988).
Omaru, A., Nagamine, M. and Nakajima, N. (Sony Corp.), US Patent 5451477 (1995).
Prest, Jr., W. M. and Luca, D. J., "The Formation of the γ Phase from the α and β Polymorphs of Polyvinylidene Fluoride," *J. Appl. Phys.*, **49**, 5042 (1978).
Rosenberg, Y., Sigmann, A., Narkis, M. and Shkolnik, S., "The Sol/Gel Contribution to the Behavior of γ-Irradiated Poly(vinylidene fluoride)," *J. Appl. Polym. Sci.*, **43**, 535 (1991).
Sajkiewicz, P., "Crystallization Behavior of Poly(vinylidene fluoride)," *Eur. Polym. J.*, **35**, 1581 (1999).
Sato, Y., Wada, R., Tazaki, M. and Okabe, M., "Gelation Process of Poly(vinylidene fluoride)/Cyclohexane Solution," *Nihon Kagaku Kaishi*, 481 (1998).
Sugawara, S., "Polymer Binder in Lithium-ion Rechargeable Battery," Advanced Technologies for Polymer Battery, Oyama, N., ed., CMC Press, Chap.6 (1998).
Tazaki, M., Wada, R., Okabe, M. and Homma, T., "Crystallization and Gelation of Poly(vinylidene fluoride) in Organic Solvents," *J. Appl. Polym. Sci.*, **65**, 1517 (1997).
Voice, A. M., Davies, G. R. and Ward, I. M., "Structure of Poly(vinylidene fluoride) Gel Electrolytes," *Polym. Gels Networks*, **5**, 123 (1997).